Chapter 5
Void Formation by Kirkendall Effect in Solder Joints

M. J. M. Hermans and M. H. Biglari

5.1 Diffusion

With diffusion, the atomic movement within a solution is meant. Diffusion can be treated either as an atomistic or as a continuum approach. In the former, the nature of the diffusing species is considered on an atomic level, whereas the latter the system is treated as a continuous medium on a more micro- and macroscopic level.

Diffusion may occur by migrating of interstitial or substitutional atoms, depending on the sites the atoms occupy in the lattice.

Usually the concentration of interstitial atoms is small and only a fraction of the available sites is occupied. This means that there are always neighboring site where the interstitial atom can jump to. For substitutional atoms, vacancies must be present in the lattice.

Assume an ideal solid solution with A, the solute component, and B, the solvent component. Due to vacancy motion, atoms can move through the lattice and the probability for jumping into the vacancy is the same for all the atoms surrounding the vacancy. This implies that the jump rate does not depend on the concentration.

When a concentration gradient exists within the solution, there will be a net flux of atoms down the concentration gradient. For a one-dimensional system, this flux can be described by Fick's fist law of diffusion:

$$J_A = -D_A \frac{\mathrm{d}C_A}{\mathrm{d}x} \tag{5.1}$$

M. J. M. Hermans (✉)
Delft University of Technology, Materials Science and Engineering Joining and Mechanical Behaviour, Mekelweg 2, Delft, The Netherlands
e-mail: m.j.m.hermans@tudelft.nl

M. H. Biglari
Mat-Tech BV, Ekkersrijt 4605, Eindhoven, The Netherlands
e-mail: m.biglari@mat-tech.com

G. Grossmann and C. Zardini (eds.), *The ELFNET Book on Failure Mechanisms, Testing Methods, and Quality Issues of Lead-Free Solder Interconnects*,
DOI: 10.1007/978-0-85729-236-0_5, © Springer-Verlag London Limited 2011

with D_A the diffusion coefficient or diffusivity and $\frac{\mathrm{d}C_A}{\mathrm{d}x}$ the concentration gradient.

The diffusion coefficient depends on the activation energy for the migration and can be expressed as:

$$D_A = \left[\frac{1}{6}\alpha^2 z v \exp\frac{\Delta S_m}{RT}\right]\exp\frac{-\Delta H_m}{RT} = D_{A0}\exp\frac{-Q}{RT} \quad (5.2)$$

with α the jump distance (Å), z the number of nearest neighbors, v the lattice vibration frequency (s^{-1}), ΔS_m the activation entropy (J mol^{-1} K^{-1}) and ΔH_m the activation enthalpy (J mol^{-1}).

Although derived for interstitial diffusion, the equations are also applicable for any diffusing specie in a cubic lattice.

For non-steady conditions, where the concentration varies with distance and time, Fick's second law of diffusion should be used.

$$\frac{\partial C_A}{\partial t} = \frac{\partial}{\partial x}\left(D_A\frac{\partial C_A}{\partial x}\right) \quad (5.3)$$

This equation relates the rate of change of composition with time to the concentration profile. When the variation of D_A with concentration can be ignored, the equation can be simplified.

$$\frac{\partial C_A}{\partial t} = D_A\frac{\partial^2 C_A}{\partial x^2} \quad (5.4)$$

It should be kept in mind that D is in solid solutions often dependent on the composition as can be seen in Fig. 5.1 for three gold alloys.

In binary substitutional alloys, the situation is more complex. The rate at which the solvent and solute atoms can move to a vacancy is not equal and each atomic species must be given its own intrinsic diffusion coefficient.

$$J_A = -D_A\frac{A\partial C_A}{\partial x} \text{ and } J_B = -D_B\frac{A\partial C_B}{\partial x} \quad (5.5)$$

J_A and J_B are the fluxes of A and B atoms across a given lattice plane (cross-sectional area A). If these fluxes are in opposite directions and when they are not equal, a net flux exists which should be matched by a flux of vacancies in the opposite direction of the net flux of atoms, see Fig. 5.2. When the vacancy concentration should be maintained near the equilibrium, vacancy concentration on one side of the interface vacancies should be created, while on the other side they should be annihilated. Jogged edge locations can provide a source and sink of vacancies. This means that extra atomic planes are introduced on one side while planes are annihilated on the other side of the interface, see Fig. 5.3. The velocity of any given plane can be related to the flux of vacancies crossing it:

$$v = (D_A - D_B)\frac{\partial X_A}{\partial x} \quad (5.6)$$

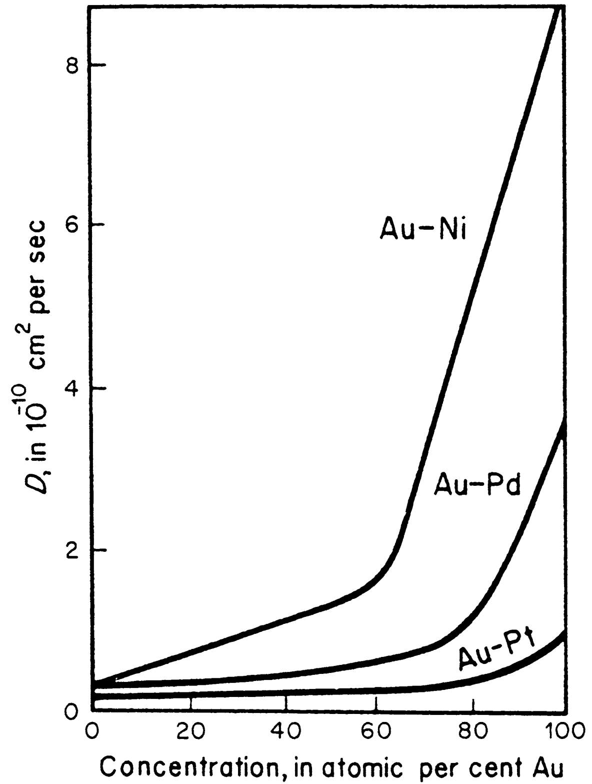

Fig. 5.1 Variation in diffusion coefficient (D) with composition for three Au alloys [2]

It can be derived that Fick's second law for diffusion in substitutional alloys is:

$$\frac{\partial C_A}{\partial t} = \frac{\partial}{\partial x}\left(\tilde{D}\frac{\partial C_A}{\partial x}\right) \tag{5.7}$$

in which $\tilde{D}$ is the interdiffusion coefficient, depending on D_A and D_B.

$$\tilde{D} = X_B D_A + X_A D_B \tag{5.8}$$

with X_A and X_B the mole fractions of A and B, respectively.

It should be mentioned that the atomic mobility along defects (grain boundaries, surfaces, dislocations) can be considerable different from bulk diffusion. A shift in diffusion path mechanism can for instance occur with varying temperature. Atomic mobility is also influenced by electromigration.

Finally, when additional diffusing species are present in the system, the diffusivities are altered as the probability of a jump into a vacancy will change.

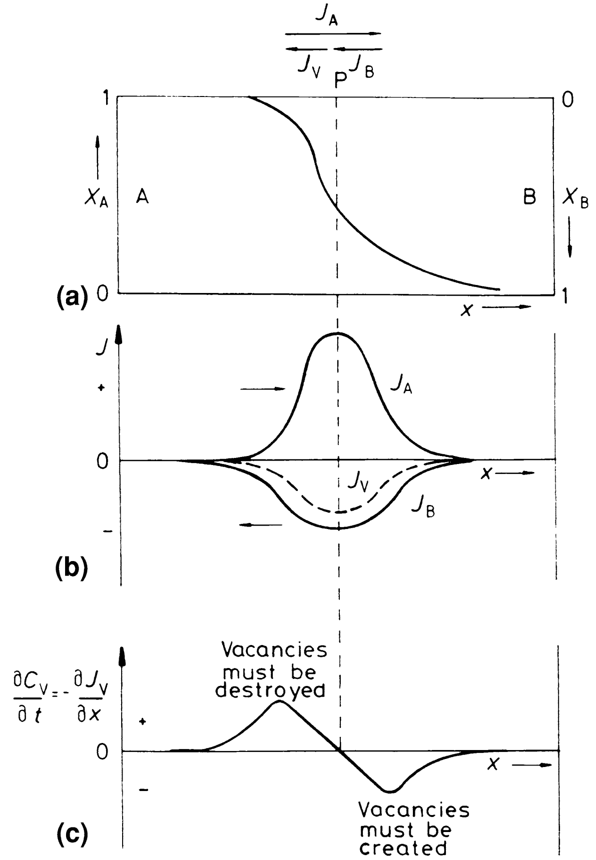

Fig. 5.2 Interdiffusion and vacancy flow [3]

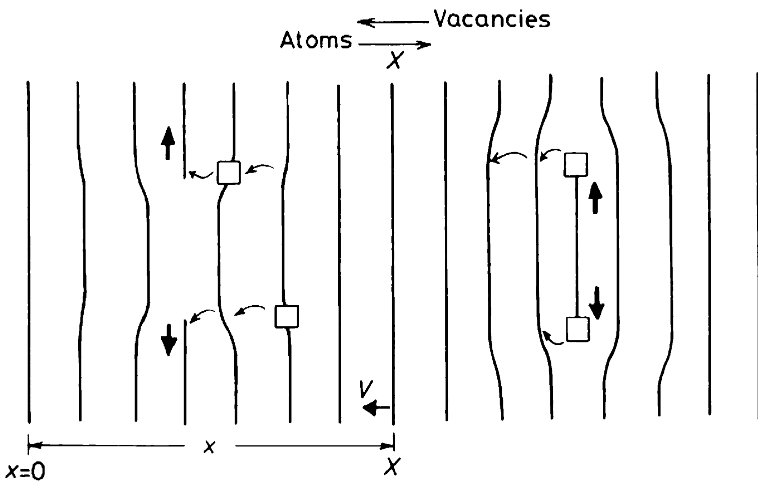

Fig. 5.3 The flux of vacancies causes the atomic planes to move through the specimen [3]

5.2 Kirkendall Effect

The experiment by Smigelskas and Kirkendall [1] studied the diffusion couple copper–zinc. At the original interface of the two pure metals, fine marker wires were incorporated. After annealing, the concentration profiles were determined across the interface. The interesting result of their study was that the marker wires had moved during the diffusion process. This is shown schematically in Fig. 5.4, where the upper figure represents the situation before the heat treatment, while the lower figure shows the position after diffusion had occurred. The distance of the marker movement was found to vary with the square root of time the specimen was kept at the diffusion temperature. The moving plane in which the markers are situated is called the Kirkendall plane.

This marker movement could only be explained by a different speed of diffusion for the different types of atoms. In this way, the effect confirms the vacancy mechanism of diffusion, with different rates of jumping into a vacancy for both types of atoms. Cooperative movement (direct interchange and Zener-ring mechanism) of atoms can be discarded in the case the Kirkendall effect is observed.

Darken's equations (Eqs. 5.6 and 5.8) makes it possible to determine the intrinsic diffusivities experimentally. The following assumptions are required for this derivation.

- volume expansion/contraction due to unequal mass flow only takes place in the direction perpendicular to the interface
- the total number of atoms per unit volume is a constant ($n_A + n_B$ = constant)
- porosity does not occur in the specimen during the diffusion process.

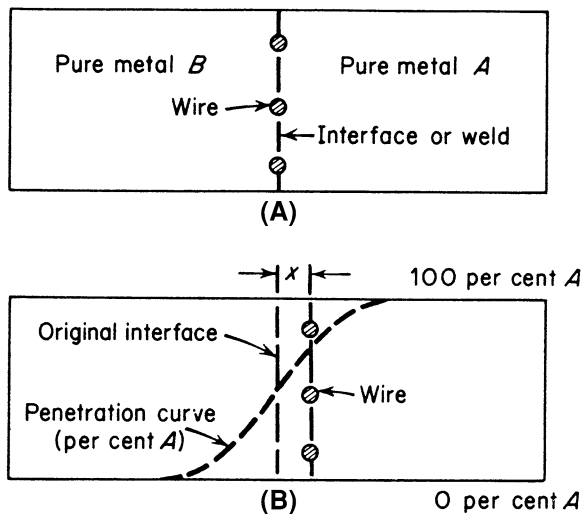

Fig. 5.4 Marker movement in a Kirkendall diffusion couple [2]

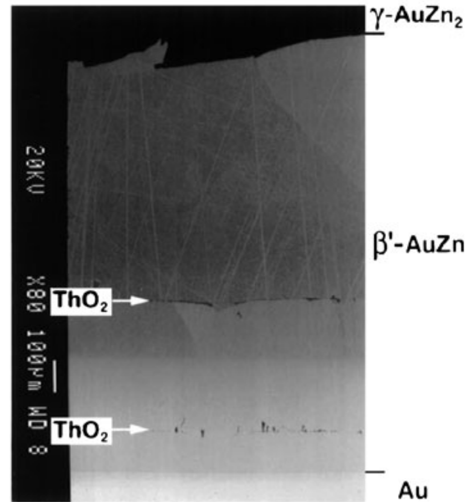

Fig. 5.5 Back-scattered electron image (BEI) of an Au_$Au_{36}Zn_{64}$ ("g-$AuZn_2$") diffusion couple annealed at 500°C for 17.25 h under flowing argon. After interdiffusion, the ThO_2 markers introduced between the couple halves are clearly visible as two distinct straight rows of inclusions [4]

Two standard methods for measuring the diffusion coefficient are:

- Diffusivity is assumed constant (Grube method)
- Diffusivity is a function of the composition (Matano method).

Van Dal et al. [4] and Paul et al. [5, 6] studied the Kirkendall effect for various diffusion couples and showed that multiple Kirkendall planes can develop. This can be seen in Fig. 5.5. The Kirkendall planes can be either stable, unstable or virtual. By using a Kirkendall velocity plot, it is possible to explain and predict the Kirkendall plane formation.

5.3 Kirkendall Void Formation

Due to the difference in diffusivity of the atoms in a binary solution, one of the components in the diffusion couple will experience a loss of mass while the other component will gain mass. As a result of the mass transfer, shrinkage and expansion will occur in the parts of the system. In this way, a state of stress is introduced in the diffusion zone. The part that suffers a loss of mass is placed under a two-dimensional tensile stress, while the side that gains mass will be placed under a compressive stress. These stress fields may bring about plastic flow.

Furthermore, if one of the components in a binary diffusion couple diffuses faster than the second component, a vacancy flux passes in the direction of the slowest component. The vacancies are both created and annihilated in the metal couple at sources and sinks such as dislocations or internal interfaces, as mentioned before. The combination of vacancy flow and vacancy condensation in combination with a state of tensile stress makes it possible that voids are formed, see Fig. 5.6.

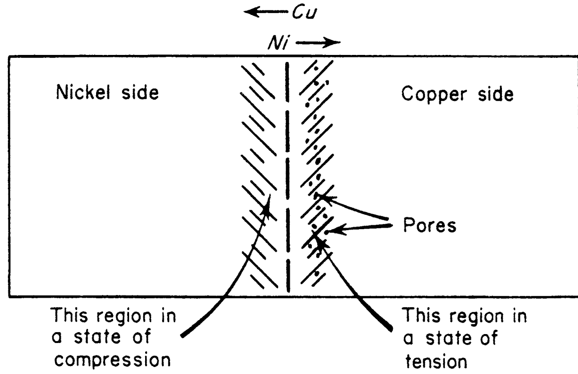

Fig. 5.6 Regions of compression and tension in a Ni-Cu diffusion couple. The formation of pores in the region in a state of tension [2]

5.4 Kirkendall Voids in Solder Joints

The evolution of the microstructure of a soldered joint is governed by the phenomena that take place during the soldering stage, where dissolution of components in the liquid metal occurs, and the subsequent solid state diffusion during its life time.

Over the last decade, effort has been undertaken to model the microstructural evolution and the occurrence of Kirkendall planes [7]. The phases can be predicted from thermodynamics and kinetics. Also the morphology of the phases plays an important role as it may influence diffusion.

It should be noted that in the case of one of the diffusion elements in the diffusion couple is deposited as a thin film, the layer may finally be completely consumed during the process, and underlying species may start to participate in the diffusion process.

A comprehensive overview of interfacial reactions between lead-free solders and common base materials is given by Laurila et al. [8]. In this review for a number of systems, values for the interdiffusion coefficient are given.

5.4.1 Diffusion Couple Sn/Cu

The phase diagram of the binary Sn/Cu system shows a series of peritectic reactions and several intermetallic compounds. In the lower temperature range (<415°C), the interfacial reactions of Cu with molten Sn-based solder result in the formation of Cu_3Sn (ε) and Cu_6Sn_5 (η) layers. This later IMC has a stable form η' at room temperature, but as available time for the transformation is short, the high temperature η remains as a meta-stable phase. The stable η' may form when the system operates at elevated temperatures. Apart from this ordening, the thickness of the layers grows during operation.

5.4.1.1 Reactions During Soldering: Cu Reactions with Liquid Sn

When liquid Sn comes into contact with Cu, Cu will dissolve until the solder becomes supersaturated. Locally, high concentrations of Cu can be realized at the vicinity of the liquid–Cu interface and Cu_6Sn_5 crystallites can form very fast in a more or less scallop-type of uniphase layer. In addition, a $Cu_6Sn_5 + Sn$ two-phase layer may form. The formation of Cu_3Sn (ε) requires long contact times and the thickness of the layer, when observed is much smaller. The morphology of the phases depends on the concentration gradients, distribution of alloying elements and cooling rates.

5.4.1.2 Reactions in the Solid State: Cu Reactions with Solid Sn

In the solid state, several temperature regimes can be addressed. Up to 60°C, only the Cu_6Sn_5 (η') phase will grow with an observable rate. The reaction is controlled by the release rate of Cu from the lattice. At room temperature, the main diffusing species is Cu. Above 60°C also Cu_3Sn (ε) will start to grow and the fraction increases with annealing time. The growth of the Cu_6Sn_5 (η) phase is controlled by the diffusion of Sn in the temperature range from 60 to 200°C. At the increased temperatures, the volume diffusion of Sn dominates over the grain boundary and interstitial diffusion of Cu. In this temperature regime, the ε phase continues to grow. The initially formed morphology of the phases during soldering will have an effect on the resulting morphology during aging.

Paul studied the intermetallic growth and the Kirkendall effect in the Cu/Sn diffusion couple [6]. Cu_6Sn_5 and Cu_3Sn layers were observed after annealing 215°C, 225 h. On the basis of the Kirkendall velocity diagram, a stable Kirkendall plane was predicted in the Cu_6Sn_5 layer. This was experimentally verified.

5.4.1.3 PbSn Solder/Electrodeposited Cu

Zeng et al. [9] studied the void formation during the reactions at the interface between eutectic PbSn solder and electrodeposited Cu. The study was initiated to the search for replacements for electroless Ni(P)/immersion gold (ENIG), which has a potential reliability issue due to 'black pad' formation. Five candidates were selected as alternative to ENIG plating: bare Cu, organic solderability preservative (OSP) on Cu, direct immersion gold (DIG) on Cu, immersion Sn on Cu and solder on Cu. They all have in common that solder will be in direct contact with Cu. The OSP will evaporate, while DIG will quickly dissolve in the solder. Sn-Cu intermetallic compounds will form during the soaking time and during aging. In this study, the microstructural development at the interface was investigated during reflow soldering (220°C) and solid state aging (up to 80 days at 150, 125 and 100°C). A large number of Kirkendall voids were observed at the interface between

Cu_3Sn and Cu. Mechanical testing (ball shear and pull) showed brittle fracture at the interface.

The microstructural development starts during the reflow process. After the flux has reduced the oxide layer, the Cu starts to dissolve in the molten solder. The layer adjacent to the interface becomes saturated with Cu. From the Sn–Pb–Cu phase diagram, the first IMC formed is Cu_6Sn_5, which forms scallop-like at the interface. The formation of the IMC takes Cu out of the saturated solder and further dissolution will take place. The phase diagram indicates that an interface between Cu and Cu_6Sn_5 is not stable and Cu_3Sn may form in between; initially, this is a very thin layer. As the Cu_6Sn_5 scallops join to become a continuous layer, the fastest diffusion routes are the channels between the scallops. If the soldering is followed by aging, the Cu_6Sn_5 scallops will transform to a layer. It is observed that the Cu_3Sn will grow faster and thicker. Kirkendall voids are introduced at the interface Cu–Cu_3Sn, see Fig. 5.7. This is observed after 3 days aging at 150°C. When aging continues, the microvoids coalesced into larger voids and finally into disk-like gaps. The number of voids did not increase significantly. The disk-like voids block the diffusion path of Cu. Without the supply of Cu, Sn becomes the fastest diffusing species, slowing down the grows of Cu_3Sn and eventually convert

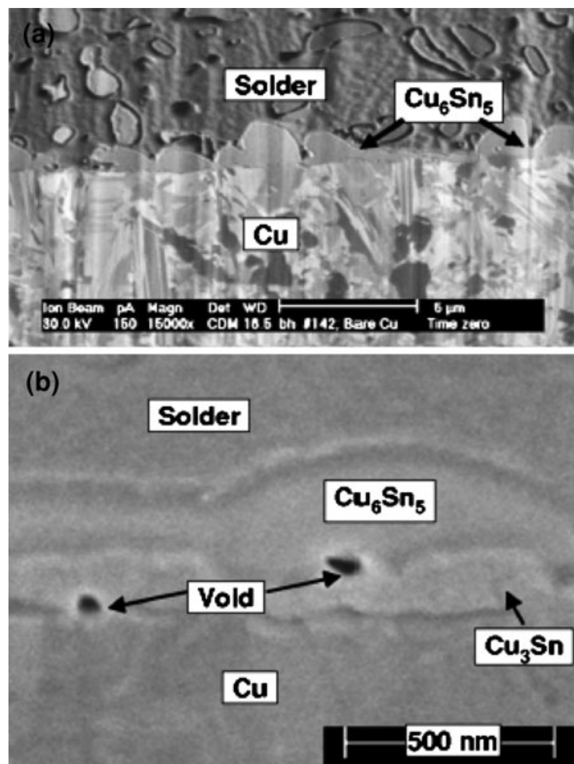

Fig. 5.7 Micrographs of cross sections through SnPb solder Cu interface after reflow of the ball attachment process (time-0), **a** ion beam image, **b** electron beam image [9]

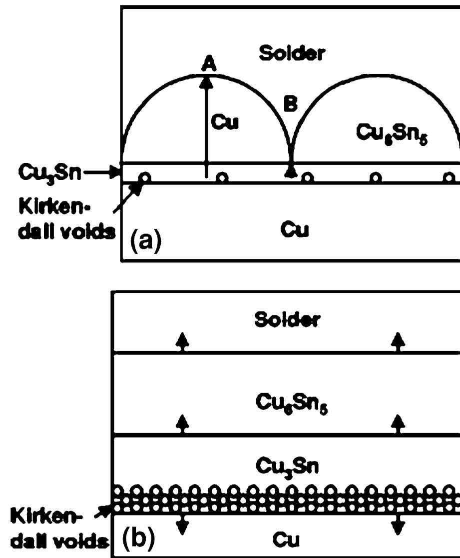

Fig. 5.8 Schematic illustration of microstructural evolution at the interface between solder and Cu: **a** after reflow; **b** after aging. The *vertical arrows* in (**a**) indicate the diffusion of Cu atoms, while those in (**b**) indicate the moving directions of the boundaries during aging [9]

it back to Cu_6Sn_5. At lower temperatures, the time required to observe the formation of voids increases.

The mechanism of the formation of the intermetallic compounds and the Kirkendall voids are schematically depicted in Fig. 5.8, in which a shows the situation after reflow and b after aging.

5.4.1.4 SnPb Solder/Sputtered Trilayer Cu/Ni(V)/Al Thin Film Metallization

Liu et al. [10] studied the reactions between eutectic SnPb solder and a sputtered trilayer Cu/Ni(V)/Al thin film metallization for UBM application, see Fig. 5.9. The initial reaction products were Cu_6Sn_5 and Cu_3Sn. The Cu layer was consumed by the Cu-Sn reaction after 1-min annealing. The scallop-type of Cu_6Sn_5 grains, in the as-received condition, grows during annealing in the direction normal to the UBM and gradually transform into a columnar morphology. At the interface Cu–Cu_3Sn, microvoids formation takes place after one reflow. The Cu_3Sn grains are grouped in clusters and Kirkendall voids are observed in the center of each cluster, see Fig. 5.10. The Cu_3Sn transforms in Cu_6Sn_5 after annealing for more than 1 min at 220°C. The Kirkendall voids that were observed to accompany the formation of Cu_3Sn disappeared when this layer transforms to Cu_6Sn_5. Cu is identified by marker movement as the dominant diffusing species and the out-diffusion of Cu is balanced by the in-diffusion of vacancies. The disappearance of the voids is explained by the diffusion of Sn through the Cu_6Sn_5 layer and the reaction with Cu_3Sn to form Cu_6Sn_5. The volume exchange between the Sn and the vacancies eventually leads to the disappearance of the voids.

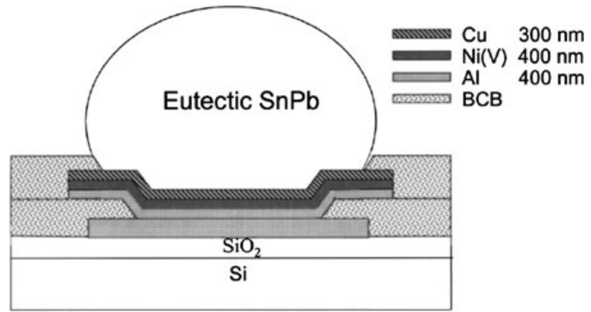

Fig. 5.9 Cross-sectional schematic representation of a SnPb solder ball on the trilayer UBM [10]

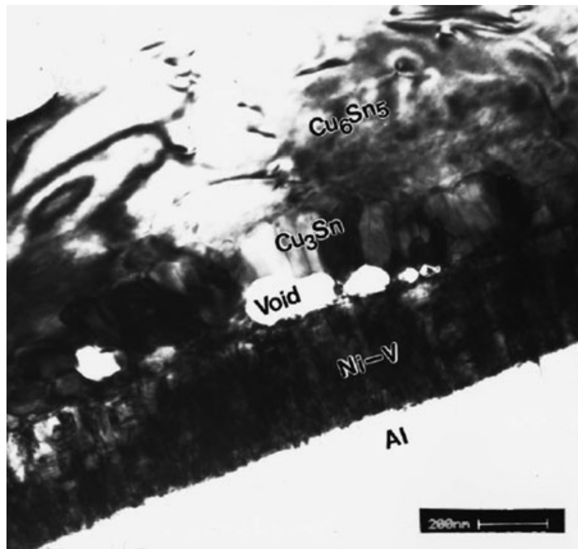

Fig. 5.10 TEM image of the Cu_3Sn grain and the Kirkendall voids [10]

The Ni(V) layer remains almost unchanged and there is no spalling of Cu_6Sn_5 and Ni(V). As the reaction between Ni(V) and solder is limited, it indicates that Cu_6Sn_5 acts as a diffusion barrier, preventing Sn to react with Ni(V).

5.4.1.5 Eutectic SnAgCu Solder/Sputtered Trilayer Cu/Ni(V)/Al Thin Film Metallization

A study was also conducted to the wetting reaction between eutectic SnAgCu and the Al/Ni(V)/Cu thin film UBM [11]. This solder shows a somewhat different behavior compared to SnPb solder as the Cu_6Sn_5 IMC does not form an optimal diffusion barrier. In fact due to the higher solubility of Cu in SnAgCu, the IMC layer dissolves. Super saturation of the solder with Cu may overcome this problem. No reference is made to the formation of Kirkendall voids.

5.4.1.6 $SnAg_{3.5}Cu_{0.7}$/CuOSP Board Metallization

Bennemann et al. [12] investigated microstructural development, IMC and defect formation in solder to package and solder to board metallization interfaces. After one reflow, the Cu_6Sn_5 and Cu_3Sn IMCs are formed. After high temperature storage, the thickness of these layers increase. Under the conditions mentioned no or only small pores are detected that were not considered to form reliability risks.

5.4.2 Diffusion Couple Sn/Ni(P)

In this section, the interaction between Sn-based solders and a Ni(P) substrate will be discussed. The interfacial reactions between Sn and Ni are described in detail by Laurila [8]. It should be noted that additional alloying components influence the evolution of the microstructure.

5.4.2.1 Sn-3.5Ag/Electroless Ni(P)

The microstructural evolution and mechanical properties were studied for soldered tensile testing specimens, as presented in Fig. 5.11a, and for UBM configurations [13, 14]. The reflow temperature was 251°C for 3 min, while the specimens were aged at different temperatures and times.

It appears that three interfacial layers are formed, Ni_3Sn_4, NiSnP and Ni_3P, as depicted in Fig. 5.11b. The as soldered specimens fracture during tensile testing in the bulk solder. Fracture position for the aged specimen gradually changes to the interface of the solder/Ni_3Sn_4, and finally to the Ni–P/Ni substrate interface, depending on temperature and time. During aging, the intermetallic compound layer thickness increases. At the later interface also, Kirkendall voids are observed inside the Ni_3P layer, see Figs. 5.12 and 5.13. Silver forms Ag_3Sn IMC particles randomly distributed inside the solder matrix. It is not likely that it has a major effect on Sn-Ni interfacial reactions.

The mechanism of the reactions of the solder with Ni–P UBM is sketched in Fig. 5.14. The formation of Ni_3Sn_4 caused a depletion of Ni in the Ni–P layer. This results in the formation of Ni_3P, which is crystalline. Growth of Ni_3Sn_4 is supposed to come from the net Ni out-flux through the Ni_3P layer. Diffusion through this layer is relatively easy due to the columnar grains. Sn does not diffuse up to the Ni_3P layer but remains in a ternary NiSnP layer.

Jeon et al. [15] found Kirkendall voids in the Ni_3Sn_4 layer close to the Ni_3P layer, both not inside this layer.

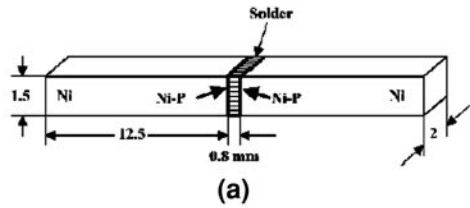

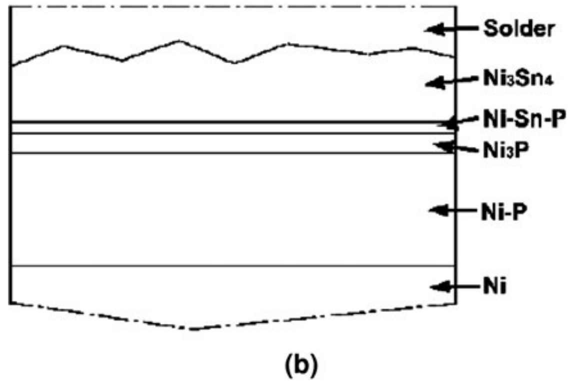

Fig. 5.11 **a** Dimensions of the tensile testing specimen used in this study. The dimensions are in millimeters, **b** Schematic diagram of the interfacial layer structure in a thermally aged Sn–3.5Ag/Ni–P solder joint [14]

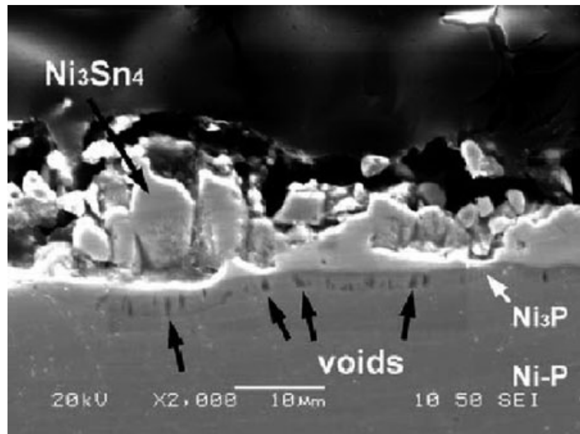

Fig. 5.12 Cross-sectional view of the magnified failure path, the failure between the solder and Ni_3Sn_4. Kirkendall voids are visible in the Ni_3P layer [14]

5.4.2.2 SnAgCu Eutectic/Ni(P)

Upon reflow at 240°C, apart from the Ni_3P layer, a $(Cu,Ni)_6Sn_5$ layer is formed rather than a Ni_3Sn_4 IMC [11]. During aging, the Ni atoms were diffusing back toward the NiSnP layer and Sn atoms were diffusing into the Ni_3P layer. Kirkendall voids were found in the NiSnP layer. Because Ni is coming from $(Cu,Ni)_6Sn_5$ to the NiSnP and no P is found in the $(Cu,Ni)_6Sn_5$, the voids should have been generated by the outward diffusion of Sn.

Research by Li et al. [16] states that $(Cu,Ni)_6Sn_4$ dominates at the interface. No Kirkendall voids are found, which can be due to the low aging temperature of 80°C.

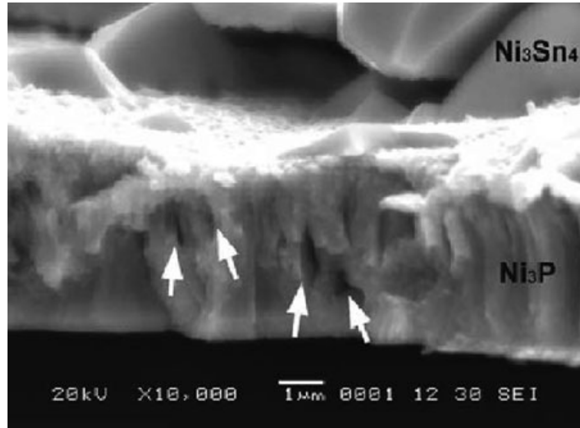

Fig. 5.13 Crack propagates through all interface layers, including the Ni_3P layer, which contains Kirkendall voids (shown by the *arrows*). The joint was aged at 190°C for 400 h [14]

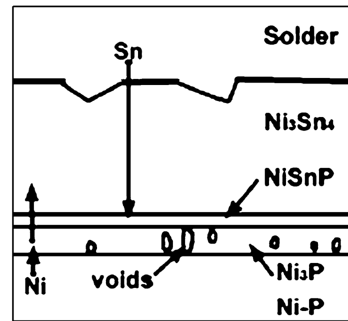

Fig. 5.14 Schematic representation of the mechanisms in Solder-Ni–P [14]

5.4.2.3 $SnAg_{3.5}Cu_{0.7}$/Electroless Ni(P) Metallization

Related work has been carried out by Benneman et al. on the microstructural development of second level interconnects using lead-free $SnAg_{3.5}Cu_{0.7}$ on an XFLGA package [12]. The interfaces solder/packaging metallization and the interface solder board metallization has been studied. The IMC morphology depends on the Ni deposition (electroless, electroplated) and the solidification. The results related to the NiAu board finish are described. Ni_3Sn_2 and Ni_3Sn_4 IMCs are observed after reflow. After high temperature storage, the Ni_3P layer shows small pores and microcracks. After 1000 temperature cycles, small defects are found in the P enriched zone.

5.4.2.4 Sn–Pb/Electroless Ni(P)

He et al. [13, 14] demonstrated that the lead in the solder decreases the activity of Sn during soldering, affecting the Sn/UBM reactions. When aging, the Pb accumulates at the interface creating a Pb-rich phase, reducing the Sn activity even

more as Sn has to diffuse through this area. In other words, IMC growth is slower when a Pb containing solder is applied.

Jang et al. [17] did not report Kirkendall voids in his experiments. He assumes decomposition of the Ni_3P layer. The Ni diffuses through the Ni_3Sn_4 layer, causing it to grow, while the P returns to the Ni–P.

Zeng et al. [9] mention that Kirkendall voids observed in the Ni_3Sn_4 layer, near the Ni_3P for eutectic SnPb solder.

5.4.3 Diffusion Couple Sn–Zn/Cu

Islam et al. [18] investigated the formation of IMC in the system Sn-Zn solder/Cu substrate during reflow and extended reflow. The formation of IMCs γ-Cu_5Zn_8, β-CuZn and an unknown thin Cu–Zn layer is found. Kirkendall voids are observed in this layer.

5.4.4 Diffusion Couple Sn/Ag

Silver dissolves relatively quickly in liquid Sn and the formation of the IMC Ag_3Sn is mentioned [8]. When AgPd metallization is used to reduce the dissolution of Ag but mechanical problem may arise due to Kirkendall voiding. The number of investigations in this system is relatively small.

5.5 Conclusions

The Kirkendall effect manifests itself by the movement of marker planes in a diffusion couple system. It is the result of a net mass flow, accompanied by a vacancy flow in the opposite direction.

A large number of studies are dedicated to the microstructural evolution in solder-substrate systems. Apart from experimental work, models are becoming available to predict the microstructures.

No reference is found to predict the formation of Kirkendall voids. The voids are observed experimentally in many diffusion couple systems, but it receives not much attention.

IMC layers with Kirkendall voids are an easy path for crack propagation and determine the reliability of the solder joint.

5.6 Appendix

See Table 5.1.

Table 5.1

Solder	Substrate	Process	Aging	IMC	Kirkendall voids	References
SnPb	Cu, OSP on Cu, DIG on Cu, imm. Sn on Cu	Reflow 220°C,	100, 125, 150°C, up to 80 days	Cu_6Sn_5, Cu_3Sn	At interface Cu_3Sn and Cu	[9]
SnAgCu	Cu/Ni(V)/Al thin film metallization	Multiple reflow 1–20	260°C, 5, 10, 20 min	Cu_6Sn_5 dissolves, Ni consumed		[11]
SnAgCu	CuOSP board metallization	Reflow 1–10 260°C	150°C, 1000 h, TCoB 1000× −40 to 125°C,	Cu_6Sn_5, Cu_3Sn	Nanoscopic defects in Cu_3Sn	[12]
Sn-37 Pb	Ni–P UBM	Reflow 1 213°C, 120 s	130, 150, 170°C, 100, 225, 400, 625 h	After reflow: Ni_3Sn_4 (more needle type), NiSnP (thin layer) and Ni_3P Ag_3Sn randomly distributed After aging: Ni_3Sn_4 layer flatter and thicker	Not for 130°C For 150°C long aging time, for 170°C short aging time In: Ni_3P layer	[13]
Sn-3.5Ag	Ni–P UBM	Reflow 1 251°C, 180 s	130, 150, 170, 190°C, 100, 225, 400, 625 h Air 216°C	Ni_3Sn_4 (more chunky type), NiSnP and Ni_3P Ag_3Sn randomly distributed After aging: Ni_3Sn_4 layer flatter and thicker, faster than SnPb	Not for 130°C For 150°C long aging time, for 170°C short aging time In: Ni_3P layer	[13]
Sn-3.5Ag	Ni–P Ni	Reflow				[14]
Sn-37 Pb	Ni–P UBM	Reflow	200, 220, 240°C 1–40 min	Ni_3Sn_4, NiSnP and Ni_3P Ni_3P decomposes and P returns to Ni–P	No Aging time probably to short	[17]

Table 5.1 (continued)

Solder	Substrate	Process	Aging	IMC	Kirkendall voids	References
SnAgCu	Ni–P	Up to 5× Reflow 240°C	170°C, 64 h	$(Cu,Ni)_6Sn_5$ and Ni_3P (columnar) thin layer NiSnP	Voids in NiSnP layer	[11]
SnAgCu	Ni(P)	Reflow 1–10 260°C	150°C, 1000 h, TCoB 1000× −40°C to 125°C,	Ni_3P, Ni_3Sn_4	Non-critical voids	[12]
SnPb	Ni–P	Reflow 220°C		Ni_3Sn_4 (chunky and needle type) and Ni_3P	Yes, in Ni_3P layer after prolonged reflow	[11]
Sn_9Zn	Cu	Reflow 230°C 5, 10, 20 min		γ Cu_5Zn_8, β CuZn and unknown CuZn layer	In Cu–Zn layer	[18]
Sn_8Zn_3Bi	Cu	Reflow 230°C 5, 10, 20 min		Additional Bi precipitates	In Cu–Zn layer	[18]

References

1. Smigelskas AD, Kirkendall EO (1947) Trans AIME 171:130
2. Reed-Hill RE (1973) Physical metallurgical principles, 2nd edn. D. Van Nostrand Company, ISBN 0-442-06864-6, pp 378–406
3. Porter DA, Easterling, KE (1981) Phase transformations in metals and Alloys, 1st edn. Van Nostrand Reinhold, ISBN 0-442-30439-0
4. van Dal MJH, Gusak AM, Cserhati C, Kodentsov AA, van Loo FJJ (2001) Microstructural stability of the Kirkendall plane in solid state diffusion. Phys Rev Lett 86(15):3352–3355
5. Paul A, van Dal MJH, Kodentsov AA, van Loo FJJ (2004) The Kirkeldall effect in multiphase diffusion. Acta Mater 52:623–630
6. Paul A (2004) The Kirkendall effect in solid state diffusion, PhD thesis, Eindhoven University of Technology, ISBN 90-386-2646-0
7. Roönkä K, van Loo FJJ, Kivilahti JK (1998) A diffusion-kinetic model for predicting solder/conductor interactions in high density interconnections. Metal Mater Trans 29A:2951
8. Laurila T, Vuorinen V, Kivilahti JK (2005) Interfacial reactions between lead-free solders and common base materials. Mater Sci Eng R 49:1–60
9. Zeng K, Stierman R, Chiu T, Edwards D, Ano K, Tu KN (2005) Kirkendall void formation in eutectic SnPb solder joints on bare Cu and its effect on joint reliability. J Appl Phys 97:024508
10. Liu CY, Tu KN, Sheng TT, Tung CH, Frear DR, Elenius P (2000) Electron microscopy study of interfacial reaction between eutectic SnPb and Cu/Ni(V)/Al thin film metallization. J Appl Phys 87(2):750–754
11. Zeng K, Tu KN (2002) Six cases of reliability study of Pb-free solder joints in electronic packaging technology. Mater Sci Eng R38:55–105
12. Benneman S, Graff A, Schischka J, Petzold M, Theuss H, Dangelmaier J, Pressel K (2006) A SEM and TEM study of the interconnect microstructure and reliability for a new XFLGA package, 1st Electronics System integration Technology Conference, Dresden Germany, 5th–7th September 2006, 26–34
13. He M, Chen Z, Qi G (2004) Solid state interfacial reaction of Sn–37Pb and Sn–3.5Ag solders with Ni–P under bump metallization. Acta Mater 52:2047–2056
14. He M, Chen Z, Qi GJ (2005) Mechanical strength of thermally aged Sn–3.5Ag/Ni-P Solder joints. Metal Mater Trans A 36A:65–75
15. Jeon YD, Paik KW, Bok KS, Choi WS, Cho CL (2001) Studies on Ni–Sn intermetallic compound and P-rich Ni layer at the electroless nickel UBM solder interface and their effects on flip chip solder reliability. In: Electronic components and technology conference, IEEE
16. Li D, Liu C, Conway PP (2005) Characteristics of intermetallics and micromechanical properties during thermal ageing of Sn–Ag–Cu flip-chip solder interconnects. Mater Sci Eng A 391:95–103
17. Jang JW, Kim PG, Tu KN, Frear DR, Thompson P (1999) Solder reaction-assisted crystallization of electroless Ni–P under bump metallization in low cost flip chip technology. J Appl Phys 85(12):8456–8463
18. Islam MN, Chan YC, Rizvi MJ, Jillek W (2005) Investigations of interfacial reactions of Sn–Zn based and Sn–Ag–Cu lead-free solder alloys as replacement for Sn–Pb solder. J Alloy Compd 400:136–144